Hydrol. Earth Syst. Sci. Discuss., 12, 1765–1808, 2015
www.hydrol-earth-syst-sci-discuss.net/12/1765/2015/
doi:10.5194/hessd-12-1765-2015

Hydrology and Earth System Sciences
Open Access
Discussions

5 year radar-based rainfall statistics: disturbances analysis and development of a post-correction scheme for the German radar composite

A. Wagner[1], **J. Seltmann**[2], **and H. Kunstmann**[1,3]

[1]University of Augsburg, Institute for Geography, Regional Climate and Hydrology, Augsburg, Germany
[2]German Meteorological Service (DWD), Meteor. Observatory, Hohenpeissenberg, Germany
[3]Karlsruhe Institute of Technology, Institute for Meteorology and Climate Research IMK-IFU, Garmisch-Partenkirchen, Germany

Received: 18 December 2014 – Accepted: 20 January 2015 – Published: 6 February 2015

Correspondence to: A. Wagner (andreas.wagner@geo.uni-augsburg.de)

Published by Copernicus Publications on behalf of the European Geosciences Union.

Abstract

A radar-based rainfall statistic demands high quality data that provide realistic precipitation amounts in space and time. Instead of correcting single radar images, we developed a post-correction scheme for long-term composite radar data that corrects corrupted areas, but preserves the original precipitation patterns.

The post-correction scheme is based on a 5 year statistical analysis of radar composite data and its constituents. The accumulation of radar images reveals artificial effects that are not visible in the individual radar images. Some of them are already inherent to single radar data such as the effect of increasing beam height, beam blockage or clutter remnants. More artificial effects are introduced in the process of compositing such as sharp gradients at the boundaries of overlapping areas due to different beam heights and resolution. The cause of these disturbances, their behaviour with respect to reflectivity level, season or altitude is analysed based on time-series of two radar products: the single radar reflectivity product PX for each of the 16 radar systems of the German Meteorological Service (DWD) for the time span 2000 to 2006 and the radar composite product RX of DWD from 2005 through to 2009. These statistics result in additional quality information on radar data that is not available elsewhere.

The resulting robust characteristics of disturbances, e.g. the dependency of the frequencies of occurrence of radar reflectivities on beam height, are then used as a basis for the post-correction algorithm. The scheme comprises corrections for shading effects and speckles, such as clutter remnants or overfiltering, as well as for systematic differences in frequencies of occurrence of radar reflectivities between the near and the far ranges of individual radar sites. An adjustment to rain gauges is also included.

Applying this correction, the Root-Mean-Square-Error for the comparison of radar derived annual rain amounts with rain gauge data decreases from 1181 to 171 mm a^{-1} (application period: 2005, 2006 and 2009) and from 317 to 178 mm a^{-1} (validation period: 2007, 2008). The entire correction scheme is applicable on an annual scale. The correction of mean annual rain amounts derived from radar composite data for the

HESSD
12, 1765–1808, 2015

whole period leads to an almost undisturbed and homogeneous distribution of rain amounts for Germany.

1 Introduction

In literature, there is a wide range of precipitation climatologies, extending from the investigation of mean values to extreme value analysis. Gauge data as well as weather radar data provide appropriate data bases. Gauge data are suited for investigations that focus on the local precipitation depth, e.g. in extreme value analyses. The advantages of radar data are the spatial resolution and the geographical coverage. Accordingly, long-term radar data possesses a high potential for analyses which aim at precipitation patterns such as the occurrence of convective cells or the spatial distribution of intense precipitation. A variety of radar products based on cell-tracking algorithms exists which provides this information, e.g. TITAN (Dixon and Wiener, 1993), KONRAD (Lang, 2001), SCIT (Johnson et al., 1998), CELLTRACK (Kyznarova and Novak, 2009) or TRACE3D (Handwerker, 2002). These products are called secondary radar products as they extract certain information from a (primary) product or from radar based data. The advantage of these secondary radar products is that besides the intended nowcasting of convective cells a large variety of information on convective cells like cell-tracks, intense precipitation warnings or storm warnings is readily prepared. This information can be statistically analysed e.g. with the goal of establishing hazard maps. Goudenhoofdt and Delobbe (2013) show a comprehensive statistical analysis of convective storms based on 10 years of volumetric radar data processed by TITAN. Other investigations of a radar climatology for extreme rainfall can be found in Overeem et al. (2010), Wagner et al. (2006) and Bellon and Zawadzki (2003). Fabry et al. (2013) give a short overview of what is possible regarding climatologies of radar composites and typical problems that arise.

A radar climatology demands a high degree of data quality and homogeneity as often only small differences among spatial patterns are analysed. Any disturbances of these

HESSD
12, 1765–1808, 2015

patterns may lead to misinterpretations and incorrect regional distinctions. A huge variety of sources of errors for radar data exists. The uncertainty of deriving rain amounts from radar measurements using a Z/R relationship is well known (Uijlenhoet et al., 2003; Steiner et al., 2004). Errors of comparable magnitudes may be induced by the influence of the melting layer (*Bright Band*) affecting huge parts of the radar image (Fabry and Zawadzki, 1995; Franco et al., 2006; Joss and Lee, 1995; Kitchen et al., 1994; Koistinen, 1991; Krajewski et al., 2010; Sánchez-Diezma et al., 2000; Vignal et al., 1999), especially in the temperate zone. Attenuation behind strong convective cells, shading effects of buildings or mountains and artificial effects such as interfering transmitters, the sun and dual PRF second-trip echoes lead to spokes in radar images. Non-meteorological echoes caused by birds, insects, airplanes, ships or windmills usually affect single pixel or a couple of pixels. Additionally, the geometry of weather radar measurements has a significant influence on the quality and the comparability of radar range-bins within one image. On the one hand, variations that are induced by natural differences of reflectivity and rain amounts at different altitudes, partial beam-filling, overshooting and transition from snow into rain are intensified by varying beam-width and increasing altitudes of range-bins with distance from the radar site. On the other hand, the probability that a radar pixel is influenced by shading or attenuation increases with distance from the radar site.

Regarding radar composite data additional effects that are produced by the compositing algorithm or by inconsistent calibrations of radar systems have to be taken into account. One possible source of error in composite data is non-identical radar hardware. But even if the same radar systems are used, the radar availability and calibration may differ slightly. Various calibration techniques exist, e.g. using the sun (Holleman et al., 2010) or a setup of disdrometers combined with a vertical weather radar beam (Frech, 2013). The main source of error emerges from the compositing algorithm itself. For the German radar composite RX, the range-bins of the single radar measurements in polar coordinates are projected to the Cartesian system of the composite. Moreover, additional problems arise in overlapping areas of two or more radar systems, due to

HESSD
12, 1765–1808, 2015

the maximum criterion used by DWD or to different beam heights at the boundaries. That is why overlapping areas are analysed separately from single radar areas. Because of these problems, the data quality of uncorrected radar products is usually not high enough to provide a reliable basis for a radar climatology so additional corrections are required. Advanced correction algorithms on single radar images are very flexible, taking into account the current weather situation and may correct single effects like attenuation or clutter-effects from non-meteorological echoes. Different correction algorithms exist which try to reconstruct the true rain patterns in clutter affected areas (Park and Berenguer, 2013; Anderson-Frey and Fabry, 2013). These authors, additionally to the adjacent uncorrupted pixels of one radar image, also take into account the previous and the following radar images. In this way a spatial and temporal interpolation is realised. Many studies rely on the corrections on single radar images only, even for a radar climatology (Overeem et al., 2009). But for a radar climatology there is a risk that small remaining deviations may be accumulated for a longer timescale and lead to major errors (Holleman, 2007; Wagner et al., 2012). Furthermore, some corrections are not applied in DWD, e.g. VRP-correction algorithms for single radar data or composite data (Koistinen et al., 2003). So roughly all deviations resulting from increasing beam-width and increasing altitudes of radar range-bins still exist in these products. For secondary radar products a re-processing of corrected reflectivity data is usually not possible and the correction algorithms for single radar images are often not applicable to secondary radar products. Regarding radar composites additional corrections are necessary.

To overcome these problems we developed a post-correction algorithm. The approach is to focus on the total of disturbances within composite data and not on disturbances in single images. So the mean systematic variations within composite data are corrected this way. This includes frequently occurring disturbances. A statistical analysis of disturbances within accumulated radar data for several years is required as such corrections are not physically based. The aim of this analysis is to identify disturbances and investigate their spatial and temporal behaviour. Knowing the characteristics of

HESSD
12, 1765–1808, 2015

these disturbances, dependencies such as the relationship between rain amounts and beam elevation is used within the correction scheme.

The post-correction scheme is based on these results. It has been developed for long-term radar data to correct disturbed areas preserving the true precipitation patterns as far as possible. The proposed scheme is not a substitute for common correction algorithms on single radar images, but may become an additional valuable means of correction for radar climatology, especially if the analysed product still has some limitations in quality because of missing correction schemes.

The article is organised as follows: the radar data, the validation data and the investigation area are presented in Sect. 2. In Sect. 3 the statistical analysis of disturbances within radar data is described, including the used method and the main assumptions. The findings of the statistical analysis are used to develop a post-correction algorithm for a radar climatology. The method and the validation of the correction scheme with the help of interpolated rain gauge data are presented in Sect. 4.

2 Data

The investigation area is the whole of Germany with the Alps in the very southern part, the Central German Uplands in the southern and mid parts and the Northern Lowland with the coasts of the Baltic Sea and the North Sea.

2.1 Radar composite RX

This area is covered by the German radar composite RX, a mosaic of 16 operational dopplerised C-Band weather radar systems of the German Meteorological Service.

In Table 1 an overview of important local specifics of the 16 contributing German radar sites is given. The name and abbreviation of the radar site is used to identify the radar site. The altitude of the site and the minimum and maximum radar elevation at a distance of 128 km from the radar site allows to interpret differences within the com-

HESSD
12, 1765–1808, 2015

posite. Each weather radar run the same scan pattern: a volume scan consisting of 23 elevations (18 Doppler scans with dual PRF and 5 intensity scans with 250 km range) every 15 min and a terrain-following precipitation scan with 128 km range every 5 min. The RX product with 256 classes (−31.5 to 95.5 dBZ) has a resolution of 0.5 dB. It is based on the terrain-following precipitation scan of up to 16 radar systems and displays a high temporal and spatial resolution (5 min; 1 km × 1 km) projected on a 900 × 900 Cartesian grid. This product has been continuously available since 2004/2005. The evaluation period for this product lasts from 2005 to 2009. In Fig. 1 the whole coverage of the RX radar composite is illustrated. The maximum ranges of each of the 16 contributing radar systems are marked by black rings, the location of the sites are represented by its abbreviation in white letters. The colours indicate the mean altitude of each composite pixel above the radar site. For the comparison of two radar systems the altitude of each radar site has to be taken into account, but it is neglected in this figure. The red points mark the precipitation gauges that were used for the evaluation. The yellow points represent additional rain gauge locations used for the adjustment step of the correction algorithm.

2.2 Single radar product PX

A second radar product which is analysed is the local reflectivity product PX with six levels and a spatial resolution of 1 km × 1 km. A threshold of 1 dBZ in winter and 7 dBZ in summer is used for level 1 (see Table 2). It is also based on the precipitation scan with an availability every 5 min since the year 2000 for all radar sites. The evaluation range was set to 100 km because until 2005 the maximum range of the PX product was only 100 km. This product is used to analyse the influence of beam-broadening and increasing altitude of radar range-bins with distance from the radar site and permanent clutter effects for each of the 16 weather radar. The evaluation period was 2000–2006. The advantage of the additional use of single radar images is that the whole radar image can be investigated so that even gradual deviations may become apparent. Further-

HESSD
12, 1765–1808, 2015

more it may be clarified if artificial patterns in composites can be explained by clutter effects in single radar images.

The raw data used to create both RX and PX products undergo the usual corrections within the signal processor, e.g. Doppler filtering (since 2004), clutter correction, speckle remover, and thresholding for noise (LOG) and signal quality (SQI). The availability of the PX product was about 80–85 % before 2006 and over 90 % afterwards.

2.3 Rain gauge data

Monthly data of 1260 rain gauges (tipping-buckets and rain collectors) from DWD for Germany were available for the adjustment of radar data and for validation purposes. These data are quality controlled according to DWD quality standards. Not all of them cover the whole period from 2005 to 2009 or accomplish additional quality controls. Additionally, the rain gauge data was manually controlled regarding limit exceedance of monthly and annual mean values and was intercompared to adjacent rain gauges. A total between 621 and 1040 rain gauges meets the above criteria, differing from year to year.

3 Analysis of disturbances in radar composites

3.1 Methods for the analysis of disturbances

Radar images, both of rain amounts as well as of frequencies of occurrence of certain radar reflectivities are accumulated for several years. The rain amounts are calculated from radar reflectivities by a three-part Z/R relationship (cf. Table 3) (Bartels et al., 2004). The resulting data are the basis for the statistical analysis and the correction algorithm, presented in the following. For the analysis of single radar images the frequencies of occurrence of radar reflectivities of the PX product derived from the 16 radar systems are used. Deviations in these images, which are not naturally induced,

HESSD
12, 1765–1808, 2015

can be ascribed to frequent clutter effects (after filtering) or systematic variations because of measuring effects. These effects are investigated in a four-step statistical analysis:

3.1.1 Step 1

The first step of the statistical analysis is to separate uncorrupted and obviously corrupted pixels in accumulated single radar images. Two groups of corrupted pixels become apparent: the first one comprises clutter pixels mainly caused by non-meteorological echoes while the second one is made up of spokes due to shading effects by obstacles near the radar site. For the clutter pixels empirical frequencies thresholds are used to obtain a first coarse separation. Then a buffer of 2 km around the identified corrupted pixel is used to spatially extend the reach of certain clutter effects. The residual pixels are further explored for corrupted pixels using histograms, empirical distributions and a manual separation by thresholds. For the separation of spokes from uncorrupted pixels all pixels of one azimuth are treated jointly as their source of error is the same. If the median of the frequency of occurrence of radar reflectivities of adjacent azimuth angles differs by more than 10 % this usually suggests a spoke, but can also easily be checked visually.

3.1.2 Step 2

The patterns of identified corrupted pixels (clutter and spokes) are explored in terms of their basic source, their temporal and spatial behaviour and in terms of the dependency on the reflectivity level, as described in Wagner et al. (2012).

3.1.3 Step 3

The uncorrupted radar pixels are inspected whether an influence of the increasing beam height and -width with distance from the radar site exists (variation with altitude). Measurements at low ranges from the radar site should be comparable to those at far

HESSD
12, 1765–1808, 2015

ranges on average. Any dependencies can be linearly addressed and are regarded as bias. Therefore, the median of frequencies of occurrence of radar reflectivities in each altitude class (one class per 100 m) is calculated and plotted vs. height. Plotting all frequencies of occurrence of radar reflectivities against height would lead to a dense point cloud as naturally induced precipitation patterns usually show variations, whereas the median provide the mean behaviour with height.

Many patterns and disturbances in radar images depend on the reflectivity level. Therefore, three reflectivity levels are chosen which represent the variety of precipitation intensities:

- level 1 for light rain (and snow)
- level 3 for moderate rain
- level 5 for heavy rain

The reliability of frequency patterns in radar images depends on the total amount of frequencies of occurrence of radar reflectivities. For level 1 the patterns are highly stable whereas for level 5 single rain events still may influence these patterns.

3.1.4 Step 4

The last step is the analysis of composite data. The disturbed and undisturbed areas were adopted from single radar analysis. Where appropriate, only those measurements are used where all single radars contribute to the composite to remove effects of radar availability. The investigation of effects of different coordinate conversion methods as well as the comparison of rain amounts between adjacent radar sites and between single radar areas and overlapping areas is only qualitatively performed. To derive the preferred allocation of pixels to one radar system within overlapping areas the dependency of frequencies of occurrence of radar reflectivities or rain amount with height is used, based on measurements. Similar to single radar measurements, the median of frequencies of occurrence of radar reflectivities of undisturbed pixels in each distance

HESSD
12, 1765–1808, 2015

class (one class per 5 km) within one overlapping area is calculated and plotted vs. height for each contributing radar system.

3.2 Results of the analysis of disturbances in radar composites

3.2.1 Investigation of single radar data PX

Clutter

In Wagner et al. (2012) a detailed analysis on clutter and variations of reflectivities with height for the Munich weather radar is presented. So only a brief description of these effects is given here, but exemplarily showing now results of the analysis of the Hamburg radar.

The influence of clutter in the accumulated radar images can be seen by a sharp gradient between single pixels or pixel groups and the adjacent radar pixels. Two counteracting processes influence the accumulated rain amounts or frequencies of occurrence of radar reflectivities, both attributed to clutter. The first one is insufficiently corrected clutter resulting in higher rain amounts and counts. The second one is thresholded data resulting in lower amounts and counts. Since 2004 Doppler IIR-filtering (Infinite Impulse Response) for clutter correction is used for all radar systems at the DWD. This correction provides good results for obstacles eliminating signals with a velocity of about $0\,\mathrm{m\,s^{-1}}$ in the Doppler spectrum. The relative power difference between the filtered and the unfiltered time series is calculated and then subtracted from the output reflectivity. If this clutter correction parameter CCOR is large, the retrieval of rain echoes fails and the measurement is discarded. As a consequence, the influence of clutter decreases with higher reflectivities which can be seen in Fig. 2. Figure 2 shows the total of frequencies of occurrence of radar reflectivities for level 1 (left), level 3 (middle) and level 5 (right) for the Hamburg radar based on the PX product from 2000 to 2006. The clutter near the radar site is mainly produced by obstacles in the city of Hamburg. The number of affected pixels decreases significantly from level 1 to level 5.

HESSD
12, 1765–1808, 2015

Clutter that is produced by moving echoes caused by insects, birds, wind turbines or ships cannot be corrected efficiently by this correction method. Additionally, ships have different cross sections, so the produced clutter is variable. For the Hamburg radar, clutter influence from ships becomes obvious at the river Elbe but only for higher reflectivities. Compared to buildings, clutter from ships is not a permanent phenomenon. So the frequencies of occurrence of radar reflectivities of each level play an important role. For high frequencies (Fig. 2, left), the ship-clutter is negligible whereas for low frequencies (Fig. 2, right) it becomes a dominant pattern.

Spokes

Different sources and types of spokes in radar images exist. Positive spokes usually originate from other emitters like the sun or from second-trip-echoes under dual PRF. But the frequency of these spokes is usually too small to become statistically significant. The spokes in Figs. 2 and 4 are negative spokes caused by shading effects behind buildings near the radar site. Only a certain part of the power is available for measurements behind these obstacles resulting in lower reflectivities. This affects all pixels of one azimuth in a similar way. So for detection, pixels of one azimuth should be regarded jointly. For the correction, a differentiation between spokes with or without rain patterns is useful. This is done visually.

Variation with altitude

The classified uncorrupted radar pixels show significant differences of frequencies of occurrence of radar reflectivities close and far from the radar site. These discrepancies are attributable to the interaction of measuring effects and natural variations of reflectivity with height. The main measuring effects are the increasing range-bin height and -size with altitude from the radar site. Natural variations are caused by the transition from snow to rain, the varying vertical extension of rain echoes or the influence of the *Bright Band*. These natural variations vary temporally and they depend on the type of

HESSD
12, 1765–1808, 2015

precipitation and on the temperature (Wagner et al., 2012). Here only the annual data of all radar sites are investigated.

Figure 3 gives an overview of the frequencies of occurrence of radar reflectivities per altitude for the Hamburg weather radar based on the accumulated PX product from 2000 to 2006 for reflectivity levels 1 (left), 3 (middle) and 5 (right). Ignoring the clutter affected inner part of the radar image, a linear decrease of the frequencies of occurrence of radar reflectivities with height becomes apparent for all reflectivity levels. This decrease with height is different for each level, ranging from 10 % km^{-1} height for level 1 to 16 % km^{-1} height for level 3 and 25 % km^{-1} height for level 5. To explain these discrepancies the interaction of meteorology and measuring effects has to be examined. Reflectivities decrease with height on average. Regarding radar measurements, a shift of frequencies results with higher reflectivities near the radar site and smaller reflectivities at far ranges. Snow and light rain only show low vertical extensions of rain echoes but usually a high horizontal homogeneity. So the dependency of the reflectivity value on height is important. Partial beam filling and overshooting results for higher altitudes. The increase of the range-bin-size with distance from the radar for small reflectivities is probably not as significant as for high ones. High reflectivities can be associated with small scale convective rain types showing a high vertical homogeneity. But often this rain type cannot be adequately resolved and leads to higher decreases at far ranges from the radar site than at low ranges. So the higher reflectivity values depend less on the altitude, but strongly on the range-bin size. For the Munich weather radar the high altitudes exclude the measurement of especially light rain types at far ranges. Additionally, the varying beam angle conceals the dependence on the range-bin size. Both effects may intensify the decrease of the frequencies of occurrence of radar reflectivities of light rain or weaken the decrease for higher reflectivities. Local differences in meteorological or radar site specific conditions like the altitude of the radar site compared to the environment may play a certain role as well. The analysis of the data derived from the 14 residual radar systems does not allow a clear interpretation.

HESSD
12, 1765–1808, 2015

3.2.2 Investigation of composite radar data RX

Figure 4 shows the mean annual rain amount for Germany based on the RX composite data from 2005 to 2009. Some particular features and anomalies become apparent that do not originate from precipitation. High "rain amounts" due to the influence of clutter close to the radar sites and negative spokes around radar sites are visible. Near the coasts of the North and Baltic Sea, lines of clutter are produced by ships. All of the radar systems reveal a greater or lesser decrease of rain amount with distance from the radar site. In addition, there are some compositing shortcomings. Adjacent radar systems e.g. the Emden radar in the very north-west of Germany and the Hamburg radar to the east of the Emden radar, show significant differences in rain amount. Furthermore, the boundaries of the overlapping areas of several radar systems are visible because of the tendency of higher rain amounts in all overlapping areas compared to single radar areas.

Figure 5 gives an overview of the main types of disturbances in the RX composite data. Single radar areas are marked white whereas overlapping areas are marked in different blue colours revealing the varying number of contributing radar systems. The yellow colour indicates the spokes which still include precipitation patterns. The red colour marks clutter.

In the following, these patterns and disturbances are analysed and evaluated that are caused by the compositing algorithm, based on the RX composite data from 2005 to 2009.

Effects of the coordinate conversion method

If several range-bins of one or more radar systems match a composite pixel, the maximum criterion is used to decide which range-bin is used. Until 2006 the so-called "push"-procedure was applied, which leads together with the maximum criterion to the extension of high range-bin values to up to 9 Cartesian pixels (Weigl and Winterrath, 2010). Besides the tendency of overestimation of reflectivity, ring structures around

HESSD
12, 1765–1808, 2015

radar sites in accumulated radar images result. In Fig. 6 the annual rain amount for the years 2005 and 2006 of the RX composite show these rings at distances of approximately 9, 25.5 and 81 km. Moving from the radar site to the outer part of the radar coverage, the rain amounts usually decrease. But when the distances of these rings are reached, the rain amounts increase abruptly. Additionally, small-scale variations of rain amounts subject to the position of the radar beam compared to the Cartesian grid are likely; they are responsible for the grainy or pixelated patterns. A correction of this effect is not considered. Since 2007 the "pull"-procedure ensures better results as only one fixed range-bin is used for each composite pixel. Only for the overlapping area of several radar sites the maximum criterion still exists.

Higher rain amounts in overlapping areas

The varying availability of radar data from different radar sites and the maximum criterion are possible reasons for the clear visibility of overlapping areas showing higher rain amounts. As to determine the effect of the maximum criterion, only those composite data are accumulated, where all radar systems contribute. The total of 518 690 measurements decreases by 29 % to 369 320 measurements in this way, even when most of the time only one radar system is missing. The availability for each radar system is usually over 90 %. Figure 4 (right) shows the mean annual rain amount for these measurements. Compared to Fig. 4 (left) no significant differences of the precipitation patterns become obvious. Again, the overlapping areas show higher rain rates than expected from the adjacent single radar areas and the sharp boundaries are visible. As a consequence, the maximum criterion seems to be mainly responsible for these patterns. In addition, the differences of rain amounts between adjacent radar systems remain. For the correction algorithm it can be concluded that the overlapping areas have to be examined and corrected separately.

HESSD
12, 1765–1808, 2015

Variation with altitude in overlapping areas

For each measurement and each pixel within overlapping areas of the composite, the maximum criterion decides which radar system provides the range-bin value. This impedes the post-correction for altitude of these areas. On average, a preferred allocation of a radar system for each pixel results. Again the decrease of the frequencies of occurrence of radar reflectivities with altitude is used to realise this allocation which has already been explained in Sect. 3.1. The intersection of two radar systems usually leads to a characteristic behaviour of the frequencies of occurrence of radar reflectivities with distance from the radar site. An example of an arbitrary overlapping area shall illustrate this behaviour: Fig. 7 shows the overlapping areas of two contributing radar systems for level 1, level 3 and level 5. The black crosses mark the frequency of occurrence of these three reflectivity levels with distance from each radar site. The red crosses indicate their median for equidistant distance classes (5 km). Pixels within the range of negative gradients imply an allocation to the considered radar system whereas positive gradients mean the opposite. The turning-point marks the transition, where it is statistically uncertain to which radar systems the measured value mainly belongs. For overlapping areas with three or four contributing weather radar systems the interpretation of the diagrams is similar. Figure 8 reveals an example for an overlapping area of three radar systems for level 3.

These gradients vary depending on the availability of the contributing radar systems and many overlapping areas are too small to derive robust values for these gradients. Fortunately, the turning points (area of transition) in Figs. 7 and 8 represent stable patterns for all levels. Knowing the areas of transition for all of the 76 overlapping areas, a map of "core-competence" for each composite pixel is derived. Figure 9 shows this map. Pixels with the same colour show a statistical derived allocation to the same radar site of more than 50 %.

HESSD
12, 1765–1808, 2015

4 Development and validation of a correction scheme

4.1 Development of a correction scheme

4.1.1 Modules of the correction scheme

Based on this knowledge of disturbance processes we design a modular concept to correct these deviations. The correction algorithm consists of four modules which have been introduced in Wagner et al., 2012: (1) the altitude correction, (2) a correction of spokes which still include precipitation patterns, (3) the adjustment to rain gauge data and (4) the correction of clutter affected pixels. The altitude correction (module 1) eliminates the effects of different elevation angles of the terrain-following scan so that the adjustment of spokes (module 2) is based on a more homogeneous data basis. For the following modules, the number of uncorrupted and corrected pixels influences the quality of the correction as those pixels were used for the adjustment to rain gauges (module 3). So it is obvious to perform this correction step directly following the altitude correction. Pixels with clutter (module 4) are corrected as a last step of the correction scheme. As these pixels are not used for adjustment in module 3, the best results are achieved when the surrounding pixels are corrected as far as possible. The single radar areas are handled separately from the overlapping areas and are discussed first. For the single radar areas the results of the single radar data analysis are checked, transferred, and if necessary modified.

4.1.2 Single radar areas

Module 1: altitude correction

The altitude correction basically corrects for systematic difference in reflectivity at close and far ranges. Here, only the net effect on an annual basis is corrected. For each of the 16 radar sites a mean decrease of frequencies of occurrence of radar reflectivities

HESSD
12, 1765–1808, 2015

with height is calculated according to Sect. 3.2.1, based on each reflectivity level of the single radar PX product. For most of the 16 radar systems, the frequency of occurrence of radar reflectivities is not only dependent on altitude, but also on reflectivity. For the correction, a gradual approach is followed: first, the linear relationship between the frequency of occurrence of radar reflectivities and altitude leads to a correction factor. Then this correction factor is varied with reflectivity.

Equation (1) shows the simple regression equation with the mean slope m and the height h. Y is the frequency of occurrence of radar reflectivities and Y_0 can be regarded as the calculated frequency of occurrence of radar reflectivities at ground level:

$$Y = m \cdot h + Y_0. \quad (1)$$

The correction factor describes the mean variation of the frequency of occurrence of radar reflectivities and can be calculated by the ratio of m and Y_0:

$$f_{\mathrm{cor}} = \frac{m}{Y_0}. \quad (2)$$

This correction factor is calculated for all of the six reflectivity levels of the PX product and for all of the 16 radar sites. Again, the variation of the correction factor with reflectivity in logarithmic scale (dBZ) can be described by a linear relationship. Reflectivity level 1 behaves slightly different from the other levels. This may partially be attributed to the higher influence of snow. Using Eq. (3), the altitude correction for each pixel results in:

$$Y_0 = \frac{Y}{(h \cdot f_{\mathrm{cor}} + 1)}. \quad (3)$$

Finally the equations are transferred to the radar composite and are slightly modified if e.g. the elevation angle of one radar system has changed since 2006. This correction is based on the frequencies of occurrence of radar reflectivities for each pixel of the single radar areas in the composite data for the years 2005, 2006 and 2009.

HESSD
12, 1765–1808, 2015

Module 2: spokes including rain patterns

The next module focuses on the correction of negative spokes which show comparable precipitation patterns as adjacent undisturbed spokes (non-zero negative spokes). Here we rely on the recognition of these spokes in the statistical analysis (see Sect. 3). The correction proceeds azimuthally by calculating the median of the rain amount or of the frequencies of occurrence of radar reflectivities for each azimuth. The median of the affected azimuth is compared to the adjacent 10 uncorrupted spokes which results in a correction factor. This correction factor is multiplied by the value of each pixel of the same azimuth. Thus, the rain pattern within a spoke is not influenced, but the blocked part of the radiation is compensated for.

Module 3: adjustment to rain gauge data

The adjustment to rain gauge data is effected in the third module. Monthly rain gauge data for the time span 2005 to 2009 were quality checked, aggregated to mean annual values and finally interpolated to the same grid as the radar composite radar data. An external drift-kriging technique based on altitude as drift variable is applied. The GSLIB libraries (Deutsch and Journel, 1992) are used for this task. Rainfall data usually have a high variation in time and in space, but on a longer temporal scale rainfall is primarily dependent on altitude. So, annual values of gauge data are interpolated. Tests show that the interpolation of monthly data leads to comparable results. But the dependency on absolute values of the altitude tends to overestimate the rain amounts at the summit locations. Better results can be achieved by using the square root of the altitude as drift-variable (Beck, 2013). The rain gauge data were converted to logarithmic values before the interpolation to get at least log-normally distributed values. This is not a mandatory precondition, but the quality and the reliability of the results of the interpolation is improved. Additionally, the estimation of the Kriging variance and the calculation of the confidence interval are deducible if the data is normally distributed. The quality of the interpolation results is closely related to the quality of the rain gauge data and to the

HESSD
12, 1765–1808, 2015

density of the monitoring network. The patterns of the terrain structure dominate the interpolated rain patterns especially if the network's density of rain gauges is low. Naturally induced variations of rain amount like windward and leeward effects cannot be adequately considered. Therefore, spatial patterns of interpolated data usually have limitations. The south-eastern part of Germany within the Alps is omitted, because the radar data is strongly affected by clutter or shading effects and the interpolated rain gauge data also show a limited reliability.

For each single radar area the median of all associated radar pixels and the median for all corresponding interpolated rain gauge pixels are calculated, compared and finally lead to an individual correction factor. In this way, radar systems that are calibrated differently are adjusted to the same independent data basis.

Module 4: clutter

The last module of the correction scheme is the distance-weighted interpolation of clutter affected pixels by surrounded pixels and is performed after the correction of the overlapping areas.

4.1.3 Overlapping areas

For the correction of the overlapping areas the same modules are used in principle, but specific modifications are performed.

Module 1: altitude correction

The altitude correction is identical to the single radar areas. But more than one radar system contributes to these areas. So the results are 2 to 4 values per pixel depending on the number of contributing radar systems. An extension of the correction algorithm is necessary, that we call the "internal adjustment" (module 3a). This also applies for the correction of spokes.

HESSD
12, 1765–1808, 2015

Module 2: spokes

Based on the results of the altitude correction, spokes are corrected in the same way for the overlapping areas as for the single radar areas. But overlapping areas and single radar areas are handled separately even though the same spoke is regarded. Each spoke can be allocated to one radar site. So it is highly likely, that within this shaded area the measurements of other overlapping radar sites have been used. This is true for spokes with and without patterns. Even though the transition area within a spoke may vary accordingly to some extent, this is neglected for the correction. This uncertainty has to be accepted as these areas are too small to be analysed in a reasonable way. The results after using this correction algorithm support this approximation (see Sect. 4.2).

Module 3a: internal adjustment

The internal adjustment aims at intersecting the multilayer results in the overlapping areas avoiding gradients. For each pixel in the overlapping area, a percentage allocation to each contributing radar system is realised, based on the map in Fig. 9. As a first approximation, the transition area between two radar systems is set to a percentage of 50 % for each radar system, whereas the pixels with the minimum distance to either radar site are set to a percentage of 100 %. The percentages of the residual pixels of the radar systems are derived by distance-weighted interpolation. These proportions are regarded to be static as long as the scan strategies did not change. Individual corrections of two or more radar systems were homogenized by using these proportions.

Module 3b: external adjustment

In case of a percentage of 100 % to one radar site for the boundary of an overlapping area, this boundary should not be visible in Fig. 4. So, the next module is the "external adjustment". It comprises more than the usual adjustment of radar data to rain

HESSD
12, 1765–1808, 2015

gauge data. The aim of the correction scheme is to avoid abrupt non-meteorologically gradients and simultaneously preserve the local rain patterns. Therefore, a stepwise adjustment to already adjusted areas is realised. Firstly, the overlapping areas of two radar systems are considered. The boundaries of overlapping areas and adjacent single radar already adjusted areas are compared. Hence, the medians of 2 to 3 rows of pixels at the boundaries are calculated and compared. In this way, a correction factor is derived for each of these boundaries. Finally, these correction factors are calculated for the whole overlapping area using the static proportions derived previously for the internal adjustment. For the external adjustment of three overlapping radar systems the single radar areas and the recently adjusted overlapping areas of two radar systems are the basis of comparison to derive the correction factors, etc. So, the correction factor includes the common adjustment to rain gauges as well as the varying percentage of contributing radar systems at the boundaries of the overlapping areas. The correction factor directly depends on the data that is to be corrected and therefore it is not static.

Module 4: clutter

The correction of clutter comprises all pixels that are massively corrupted, which means that the true rain patterns are not visible or are not reliable anymore. As a temporal interpolation is hardly possible regarding radar climatology, only a spatial interpolation is implemented considering all uncorrupted pixels within an area of 10 to 20 km around the clutter affected pixels.

4.2 Evaluation of the correction scheme

The time-series of composite radar data from 2005 to 2009 is splitted into two parts for the evaluation of the correction algorithm. The application period covers the years 2005, 2006 and 2009. The validation period is based on the data from 2007 and 2008. Data from 516 rain gauges, which are continuously available and quality proofed, are

HESSD
12, 1765–1808, 2015

the basis of comparison. On an annual basis, the rain gauge data are opposed to the rain amount derived from the spatially corresponding 9-pixel-value of the radar measurements. The 516 rain gauges applied here are a subset of the stations used for the step of adjustment of the correction algorithm and therefore are not independent from the data used for the correction (up to 1040 rain gauges). The data of the application period is used to modify the correction factors of the altitude correction for the radar composite, if necessary. The consistency between rain gauge data and radar data is shown in the scatter-plot in Fig. 10 and the Root-Mean-Square-Error (RMSE) between those two datasets is calculated. Additionally, the spatial distribution of annual rain amounts derived from uncorrected and corrected radar data is opposed to interpolated rain gauge data (basis for adjustment) in Fig. 11.

According to Fig. 10 (top), a clear relation between radar data and rain gauge is reasonable, but the dispersion is very high for the application period. A significant overestimation of annual rain amounts based on the radar data compared to rain gauge data becomes apparent. An RMSE of 1181 mm a^{-1} is calculated. For the validation period the overestimation of annual rain amounts by the radar data as well as the dispersion in the scatter plot (Fig. 10 bottom) are lower, resulting in an RMSE of only 317 mm per year. One reason for these differences may originate from the "push"-technique which was used for compositing the single radar images until 2006. This technique induces spatial inconsistencies (cf. Sect. 3.2.2) and may lead to further deviations of radar data and rain gauge data. After the correction of radar data, the RMSEs decrease to 171 mm a^{-1} for the application period and 178 mm a^{-1} for the validation period and are therefore comparable. The dispersion of pairs of values of radar data and rain gauge data in the scatter plot after the correction reveals no systematic differences between these two data sets. According to these results, the correction algorithm is also applicable to other time periods. The spatial distributions of rain amounts in Fig. 11 support this finding. The uncorrected radar data at the top show a variety of clutter effects, measuring effects and differences between radar sites. After the correction, a homogeneous distribution of rain amounts in the middle results, eliminating disturbances efficiently.

HESSD
12, 1765–1808, 2015

Minor disturbances may remain but the high consistency of rain amounts derived from radar data and from rain gauge data (bottom) becomes obvious. Certain differences between those two data sets are probable as the quality of rain gauge data and the quality of its interpolation results are also limited.

We also evaluate a more in-depth analysis of the radar data and the corresponding interpolated rain gauge data for the whole time period between 2005 and 2009. *Box and Whisker* diagrams are used to show the relative difference in percent of the annual rain amount derived from radar data and that of interpolated rain gauge data for all spatially corresponding pixels. In addition, the data sets are sub-divided spatially according to what radar site the data originated from and whether a pixel lies within an area of overlapping radar systems or within a single radar area. The allocation of pixels in overlapping areas to a certain radar site is realised according to Fig. 9. In that way, 16 plots, each containing 4 *Box–Whisker*-plots, are created. On the left hand side of each plot in Fig. 12 the pixels within single radar areas of uncorrected and corrected pairs of values are shown and on the right hand side the uncorrected and corrected pairs of values of pixels within areas of overlapping radar systems can be seen. The median is presented as a thick black line within a grey box. The grey box indicates the central 50 % of pairs of values.

Regarding the uncorrected radar data values, the plots show an overestimation of annual rain amounts for each radar site by the radar data compared to rain gauge data. The radar sites of Emden, Neuhaus, Neuheilenbach and Munich provide results of only a very slight discrepancy between both data sets. Whereas radar sites in or near bigger cities like the radar sites of Hamburg, Berlin or Frankfurt show differences of 50 % or more regarding annual rain amounts. The influence of clutter in cities plays an important role there. But clutter effects alone cannot explain the differences between adjacent radar sites. The central 50 % of radar pixels (grey box) within the single radar area of the Emden radar site show lower discrepancies to rain gauge data than the central 50 % of radar pixels of the radar site of Hamburg. The plots clearly highlight these differences among radar sites due to the causes investigated in Sect. 3.2. But

HESSD
12, 1765–1808, 2015

one also has to take into account that the size of the single radar area for each radar site in the radar composite varies.

Regarding the pixels in overlapping areas, the overestimation of rain amounts by the radar data is even more distinct, although the frequencies of occurrence of radar reflectivities and hence the rain amount decrease with range-bin height, especially within the outer parts of single radar images. As explained earlier, the maximum criterion used for compositing single radar images enhanced by the higher data availability seems to be responsible for this effect.

The median of annual rain amounts of pixels within single radar areas of corrected radar data should only show minor deviations from the corresponding rain amounts of rain gauge data because of the adjustment step. Differences can be assigned to interpolated radar pixels due to clutter effects, which are neglected for the correction step of adjustment. Pixels within overlapping areas are only adjusted at the boundaries to already adjusted areas. Nevertheless, the median of annual rain amounts of radar data and of rain gauge data shows a high consistency there. The Berlin radar site marks the maximum deviation between both data sets (+17 %), because the density of rain gauges and the number of pixels within the Berlin's radar overlapping area is low. Furthermore, differences of rain patterns between interpolated rain gauge data and measured radar data are probable.

5 Conclusions

In this study a statistical analysis of 5 years of accumulated radar composite data is presented, revealing systematic deviations within these images. A mean correction, applicable to climatological investigations, was derived from these results.

For the statistical analysis any disturbances which are already apparent within single radar images were of minor interest. The focus was on the analysis of systematic side-effects caused by the compositing algorithm, especially within the overlapping area of different radar systems. DWD's maximum criterion used for compositing results in

HESSD
12, 1765–1808, 2015

higher rain amounts within overlapping areas than in adjacent single radar areas and leads to sharp gradients at the boundaries of the overlapping areas. Additionally, the "push"-procedure, which was used until 2006, caused significant disturbances of the measured rain patterns.

Regarding the correction algorithm, the crucial point is the correction within the overlapping areas. Being a transition area from one radar site to the next, they are adjusted at each boundary to the respective adjacent single radar areas. In order to maintain the measured rain patterns, only large-scale adjustments on the basis of the median are implemented. The application of the correction algorithm shows a decrease of the RMSE from 1181 to 171 $\mathrm{mm\,a^{-1}}$ for the comparison of annual rain amounts with rain gauge data for the application period (2005, 2006 and 2009). The result of the correction algorithm is an almost undisturbed and homogeneous radar image with individual rain patterns.

The correction algorithm is designed for radar climatologies and investigations on at least an annual scale. As the algorithm is partly based on static correction coefficients or static spatial maps, the question may arise as to the impact of changing measuring settings. The correction coefficients of the altitude correction are insensitive to a modification of the scan strategy as long as the beam elevations remain in almost the same range. Such a modification of the scan strategy may influence the static map of the allocation of pixels to a single radar system. But a readjustment can easily be done, whereas a modification of the maximum range of the single radar measurements (e.g. 128 to 150 km, DWD 2010) would require elaborate adjustments: the size of the overlapping areas as well as the total amount of overlapping areas would change and therefore they would have to be re-analysed.

The correction algorithm is not only applicable to annual rain amounts but also to a selected range of rain intensities. E.g. the patterns of the distribution of intense rain may quantitatively be corrected, taking into account the ratio of the rain amount of a certain range of rain intensities and the total rain amount. A correction of frequen-

HESSD
12, 1765–1808, 2015

cies of occurrence of certain rain based measures like the frequency of occurrence of convective cells also appears feasible.

References

Anderson-Frey, A. K. and Fabry, F.: Operational mitigation of ground clutter using information from past and near-future radar scans, 36st Int. Conf. on Radar Meteor., Breckenridge, CO, AMS, 2013.

Bartels, H., Weigl, E., Reich, T., Lang, P., Wagner, A., Kohler, O., and Gerlach, N.: Projekt RADOLAN – Routineverfahren zur Online-Aneichung der Radarniederschlagsdaten mit Hilfe von automatischen Bodenniederschlagsstationen (Ombrometer), Deutscher Wetterdienst, Hydrometeorologie, available at: http://www.dwd.de/bvbw/generator/DWDWWW/Content/Wasserwirtschaft/Unsere__Leistungen/Radarniederschlagsprodukte/RADOLAN/abschlussbericht__pdf,templateId=raw,property=publicationFile.pdf/abschlussbericht_pdf.pdf (last access: 3 February 2015), 2004.

Beck, F.: Generation of Spatially Correlated Synthetic Rainfall Time Series in High Temporal Resolution: a Data Driven Approach, Mitteilungen/Institut für Wasser- und Umweltsystemmodellierung, Heft 219, Universität Stuttgart, Stuttgart, 2013.

Bellon, A. and Zawadzki, I.: A 9 year summary of radar characteristics of mesocyclonic storms and of deep convection in southern Quebec, Atmos.-Ocean, 41, 99–120, 2003.

Deutsch, C. V. and Journel, A. G., GSLIB: Geostatistical Software Library and User's Guide, Oxford University Press, New York, NY, 340 pp., 1992.

Dixon, M. and Wiener, G.: TITAN: Thunderstorm Identification, Tracking, Analysis, and Nowcasting – a radar-based methodology, J. Atmos. Ocean. Tech., 10, 785–797, 1993.

Fabry, F. and Zawadzki, I.: Long-term radar observations of the melting layer of precipitation and their interpretation, J. Atmos. Sci., 52, 838–851, 1995.

Fabry, F., Cazenave, Q., and Basivi, R.: Echo climatology, impact of cities, and initial convection studies: new horizons opened using 17 years of Conterminous US radar composites, 36st Int. Conf. on Radar Meteor., Breckenridge, CO, AMS, 2013.

Franco, M., Sánchez-Diezma, R., and Sempere-Torres, D.: Improvements in weather radar rain rate estimates using a method for identifying the vertical profile of reflectivity from volume radar scans, Meteorol. Z., 15, 521–536, 2006.

HESSD
12, 1765–1808, 2015

Frech, M.: Monitoring the data quality of the new polarimetric weather radar network of the German Meteorological Service, 36st Int. Conf. on Radar Meteor., Breckenridge, CO, AMS, 2013.
Goudenhoofdt, E. and Delobbe, L.: Statistical characteristics of convective storms in Belgium derived from volumetric weather radar observations, J. Appl. Meteorol. Clim., 52, 918–934, 2013.
Handwerker, J: Cell tracking with TRACE3D – a new algorithm, Atmos. Res., 61, 15–34, 2002.
Holleman, I.: Bias adjustment and long-term verification of radar-based precipitation estimates, Meteorol. Appl., 14, 195–203, 2007.
Holleman, I., Huuskonen, A., Kurri, M., and Beekhuis, H.: Operational monitoring of weather radar receiving chain using the sun, J. Atmos. Ocean. Tech., 27, 159–166, 2010.
Johnson, J. T., MacKeen, P. L., Witt, A., De Wayne Mitchell, E., Stumpf, G. J., Eilts, M. D., and Thomas, K. W.: The Storm Cell Identification and Tracking Algorithm: an enhanced WSR-88D Algorithm, Weather Forecast., 13, 263–276, 1998.
Joss, J. and Lee, R.: The application of radargauge comparisons to operational precipitation profile corrections, J. Appl. Meteorol., 34, 2612–2630, 1995.
Kitchen, M., Brown, R., and Davies, A. G.: Real-time correction of weather radar data for the effects of bright band, range and orographic growth in widespread precipitation, Q. J. Roy. Meteorol. Soc., 120, 1231–1254, 1994.
Koistinen, J.: Operational correction of radar rainfall errors due to vertical reflectivity profile, 25th Int. Conf. on Radar Meteor., Boston, AMS, 91–94, 1991.
Koistinen, J., Pohjola, H., and Hohti, H.: Vertical reflectivity profile classification and correction in radar composites in Finland, 31st Int. Conf. on Radar Meteor., Seattle, Washington, AMS, 534–537, 2003.
Krajewski, W. F., Vignal, B., Seo, B.-C., and Villarini, G.: Statistical model of the range- dependent error in radar-rainfall estimates due to the vertical profile of reflectivity, J. Hydrol., 402, 306–316, 2010.
Kyznarova, H. and Novak, P.: CELLTRACK – convective cell tracking algorithm and its use for deriving life cycle characteristics, Atmos. Res., 93, 317–327, 2009.
Lang, P.: Cell tracking and warning indicators derived from operational radar products, 30th Int. Conf. on Radar Meteor., Munich, Germany, AMS, 2001.
Overeem, A., Holleman, I., and Buishand, T. A.: Derivation of a 10 year radar-based climatology of rainfall, J. Appl. Meteorol., 48, 1448–1463, 2009.

HESSD
12, 1765–1808, 2015

Overeem, A., Buishand, T. A., Holleman, I., and Uijlenhoet, R.: Extreme-value modeling of areal rainfall from weather radar, Water Resour. Res., 46, W09514, doi:10.1029/2009WR008517, 2010.

Park, S. and Berenguer, M.: Reconstruction of radar reflectivity in clutter areas, 36st Int. Conf. on Radar Meteor., Breckenridge, CO, AMS, 2013.

Sánchez-Diezma, R., Zawadzki, I., and Sempere-Torres, D.: Identification of the bright band through the analysis of volumetric radar data, J. Geophys. Res., 105, 2225–2236, 2000.

Steiner, M., Smith, J. A., and Uijlenhoet, R.: A microphysical interpretation of radar reflectivity-rain rate relationships, J. Atmos. Sci., 61, 1114–1131, 2004.

Uijlenhoet, R., Steiner, M., and Smith, J. A.: Variability of raindrop size distributions in a squall line and implications for radar rainfall estimation, J. Hydrometeorol., 4, 43–61, 2003.

Vignal, B., Andrieu, H., and Creutin, J. D.: Identification of vertical profiles of reflectivity from volume scan radar data, J. Appl. Meteorol., 38, 1214–1228, 1999.

Wagner, A., Seltmann, J., and Lang, P.: URBAS_Radar – a statistical approach to radar climatology, ERAD Publ. Series Vol. 3, Abstr. 4th European Conference on Radar in Meteorology and Hydrology (ERAD4), Barcelona, Spain, available at: http://www.crahi.upc.edu/ERAD2006/proceedingsMask/00131.pdf (last access: 3 February 2015), 2006.

Wagner, A., Seltmann, J., and Kunstmann, H.: Joint statistical correction of clutters, spokes and beam height for a radar derived precipitation climatology in southern Germany, Hydrol. Earth Syst. Sci., 16, 4101–4117, doi:10.5194/hess-16-4101-2012, 2012.

Weigl, E. and Winterrath, T.: Radar based precipitation analysis and forecasting (RADOLAN, RADVOR-OP), Promet, 35, 78–86, 2010.

HESSD
12, 1765–1808, 2015

Table 1. Location of the 16 contributing radar sites of the German radar composite.

abbreviation	name	altitude [m]	MIN [m] (128 km)	MAX [m] (128 km)
HAM	Hamburg	46	2.6	2.7
ROS	Rostock	36	2.2	2.9
EMD	Emden	58	2.7	2.7
HAN	Hannover	81	2.2	3.2
UMD	Ummendorf	185	2.1	3.5
BLN	Berlin	80	2.8	2.8
ESS	Essen	180	2.8	3.0
FLD	Flechtdorf	623	2.5	2.8
DRS	Dresden	262	1.9	3.6
NEU	Neuhaus	873	1.8	2.3
NHB	Neuheilenbach	585	2.0	3.0
FRA	Frankfurt	146	2.6	4.6
EIS	Eisberg	799	1.9	2.4
TUR	Türkheim	765	2.1	3.1
MUC	München	511	3.0	5.0
FBG	Feldberg	1517	1.3	2.0

HESSD
12, 1765–1808, 2015

Table 2. Reflectivity levels of the PX product.

Reflectivity [dBZ]	1 (7)–18.9	19–27.9	28–36.9	37–45.9	46–54.9	≥ 55
Rain rate [mm h^{-1}]	0.1–1	1–3	3–9	9–27	27–80	> 80
Class	1	2	3	4	5	6

HESSD
12, 1765–1808, 2015

Table 3. Three-part Z/R relationship used to calculate rain rate from RX radar products.

Reflectivity [dBZ]	< 36.5	36.5–44	> 44
a	125	200	77
b	1.4	1.6	1.9

HESSD
12, 1765–1808, 2015

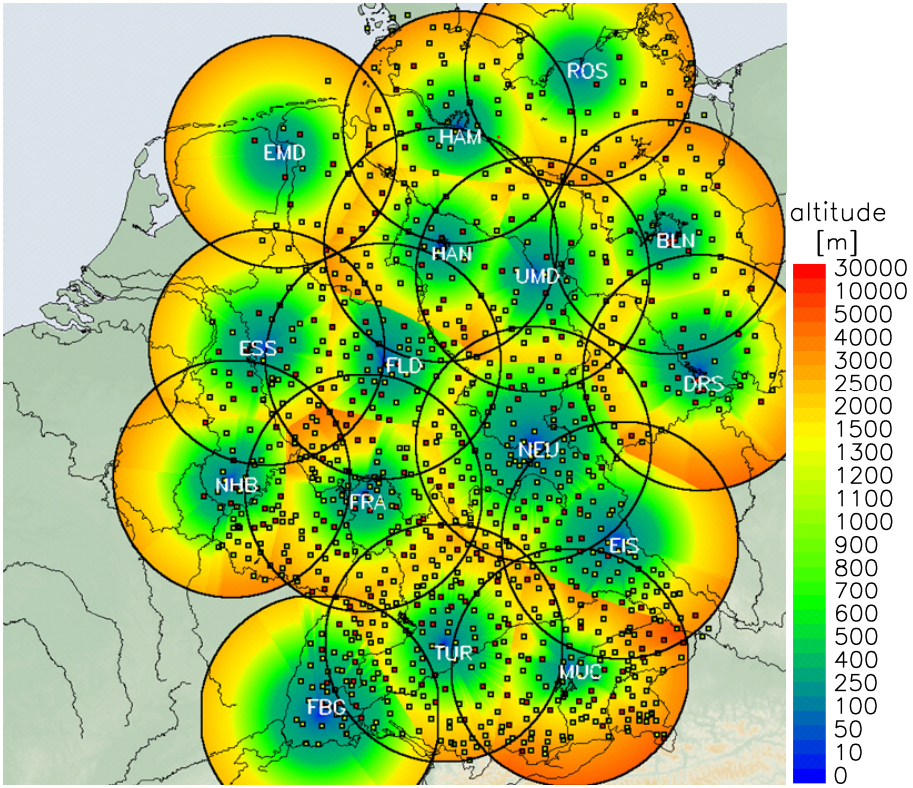

Figure 1. Mean altitudes of the near-surface precipitation scan of the 16 contributing radar sites for the German radar composite. Overplotted by locations of the rain gauges used for comparing rain amounts for the evaluation (red) and for the adjustment (red and yellow). The location of the radar sites are represented by its abbreviation in white letters.

HESSD
12, 1765–1808, 2015

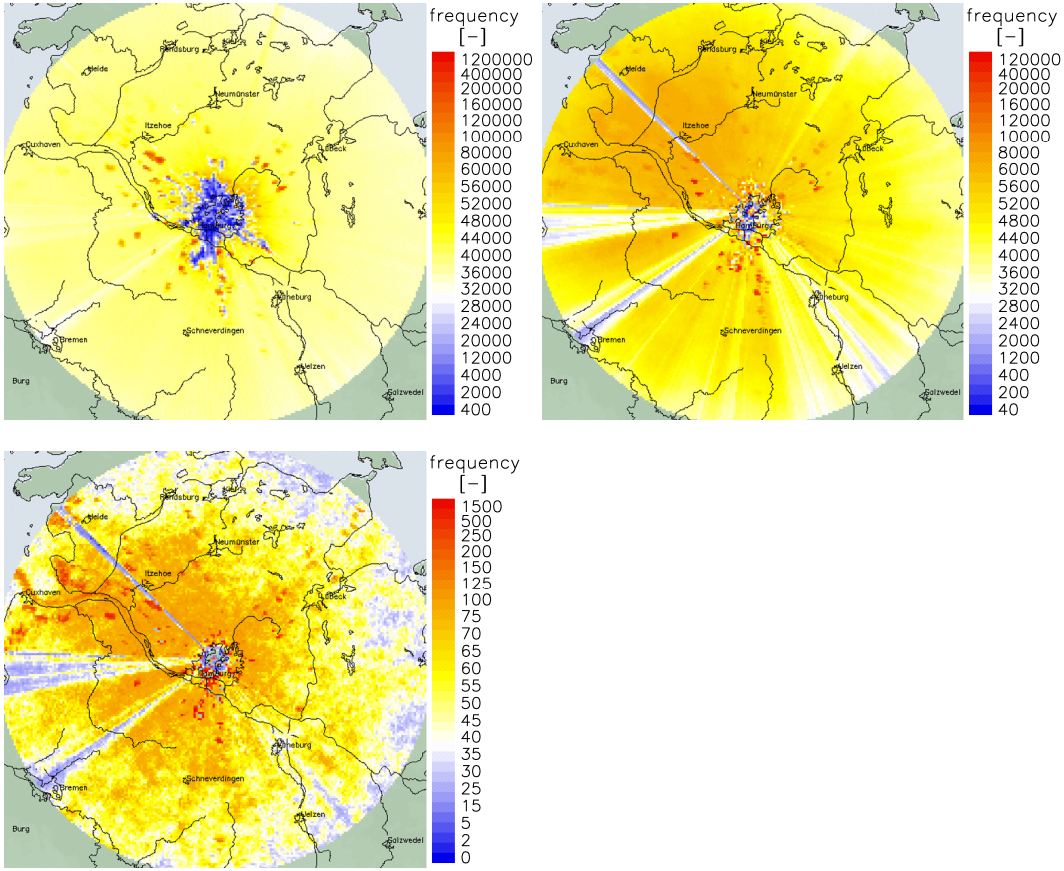

Figure 2. Uncorrected frequencies of occurrence of radar reflectivity level 1 (left panel), level 3 (middle panel) and level 5 (right panel) of the Hamburg weather radar from 2000–2006 (PX data). The scale is 200 km × 200 km.

HESSD
12, 1765–1808, 2015

5 year radar-based rainfall statistics: disturbances analysis

A. Wagner et al.

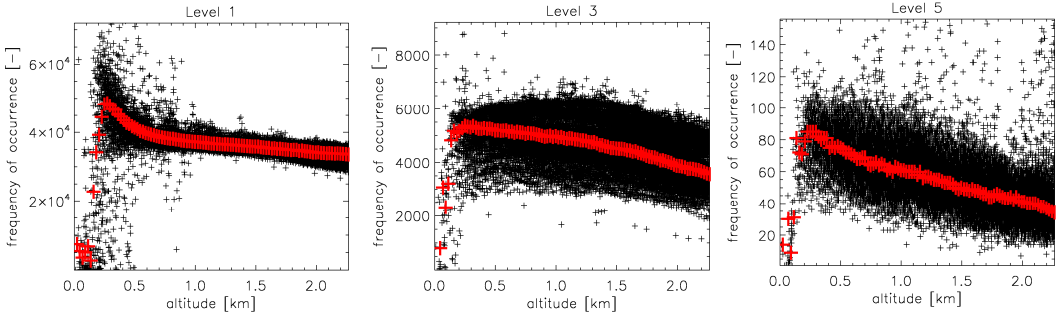

Figure 3. Characteristics of the median of the frequency of occurrence of uncorrupted pixels with height for equidistant classes of altitude for the reflectivity levels 1 (left panel), 3 (middle panel) and 5 (right panel) of the Hamburg weather radar from 2000–2006 (PX data).

HESSD
12, 1765–1808, 2015

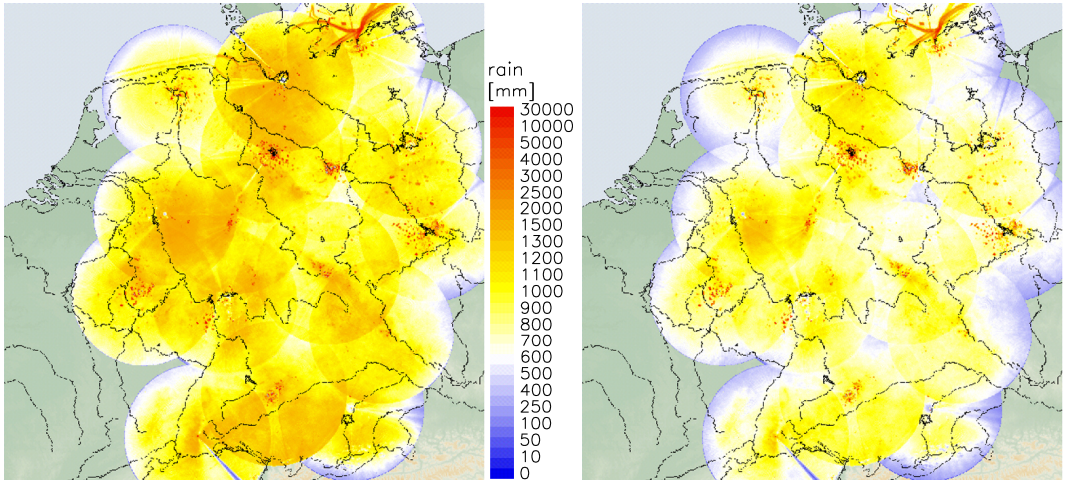

Figure 4. Uncorrected annual rain amounts for Germany based on radar composite data RX from 2005–2009 for all measurements (left) and for only those measurements where all 16 radar systems contribute. The scale is 900 km × 900 km.

HESSD
12, 1765–1808, 2015

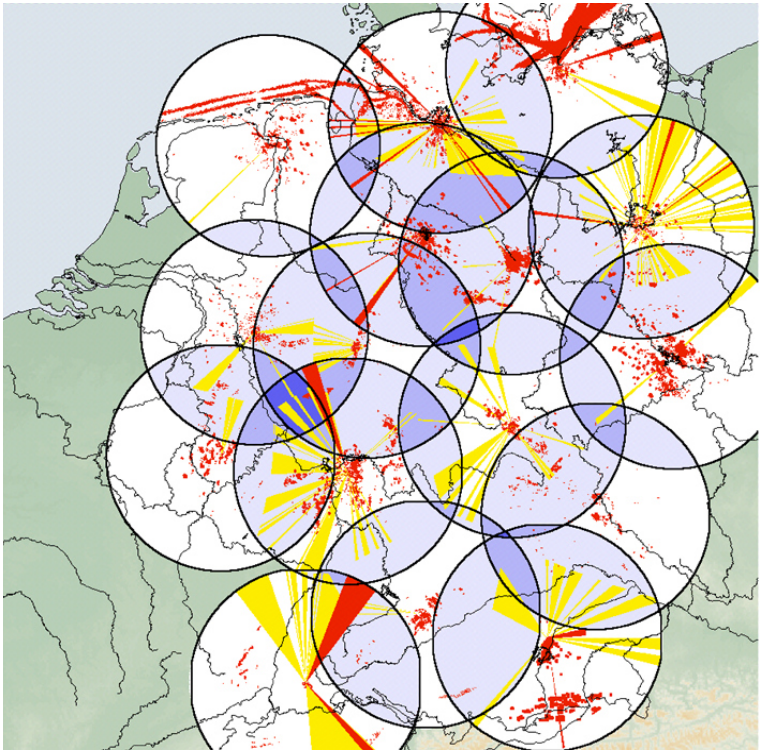

Figure 5. Overview of clutter and disturbances within the radar composite product RX including clutter pixels (red), spokes (yellow) and the overlapping areas of several radar systems in blue colours.

HESSD
12, 1765–1808, 2015

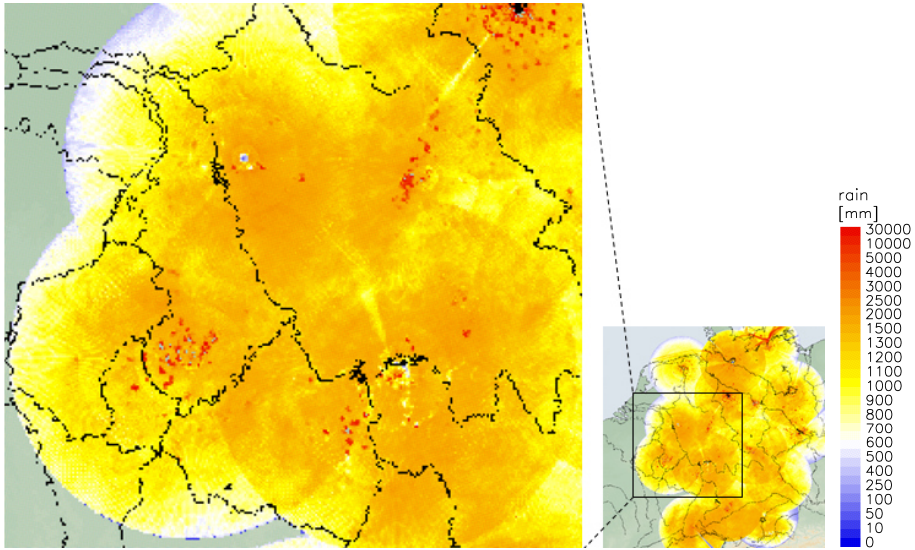

Figure 6. Image detail of the uncorrected annual rain amounts for Germany based on radar composite data RX from 2005–2006.

HESSD
12, 1765–1808, 2015

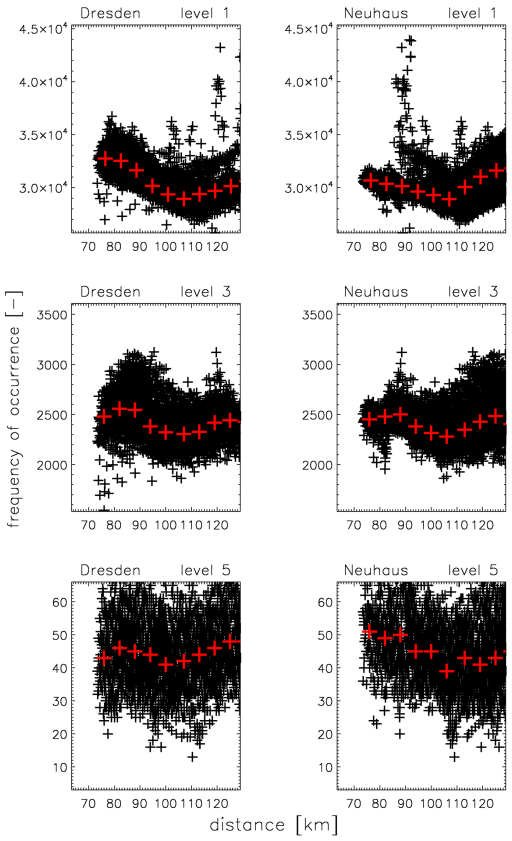

Figure 7. Characteristics of the frequency of occurrence of uncorrupted pixels with distance from the radar site for the reflectivity levels 1 (top panel), 3 (middle panel) and 5 (bottom panel) of the overlapping area of the Radar Dresden and the Radar Neuhaus for the years 2005, 2006 and 2009, overplotted by the corresponding median of equidistant classes of distance (red).

HESSD
12, 1765–1808, 2015

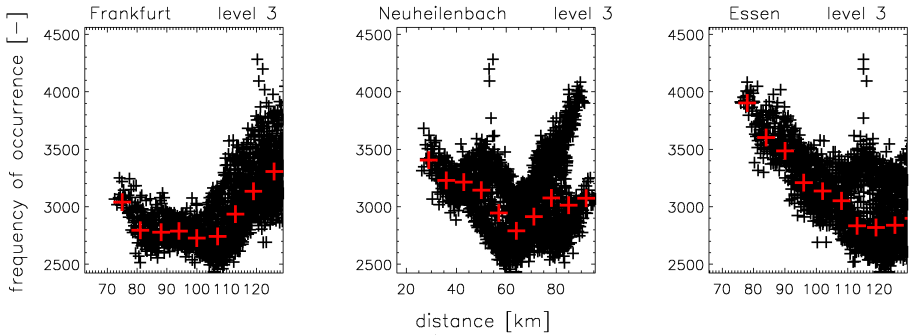

Figure 8. Characteristics of the frequency of occurrence of uncorrupted pixels with distance for the reflectivity level 3 of one overlapping area of the three weather radar systems of Frankfurt, Neuheilenbach and Essen for the years 2005, 2006 and 2009, overplotted by the corresponding median of equidistant classes of distance (red).

HESSD
12, 1765–1808, 2015

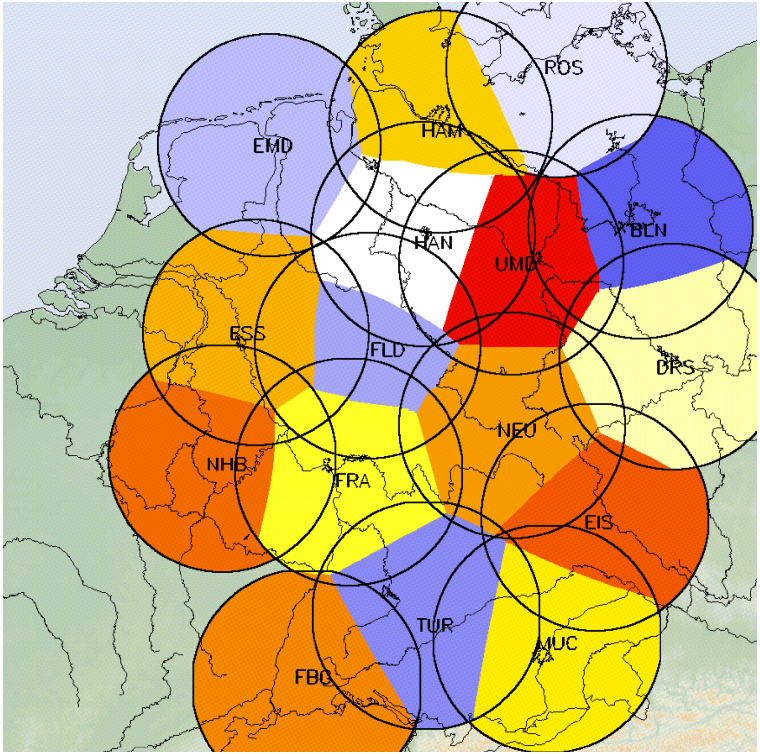

Figure 9. Mean allocation of radar pixels to radar sites within the radar composite RX. The abbreviations are explained in Table 1.

HESSD
12, 1765–1808, 2015

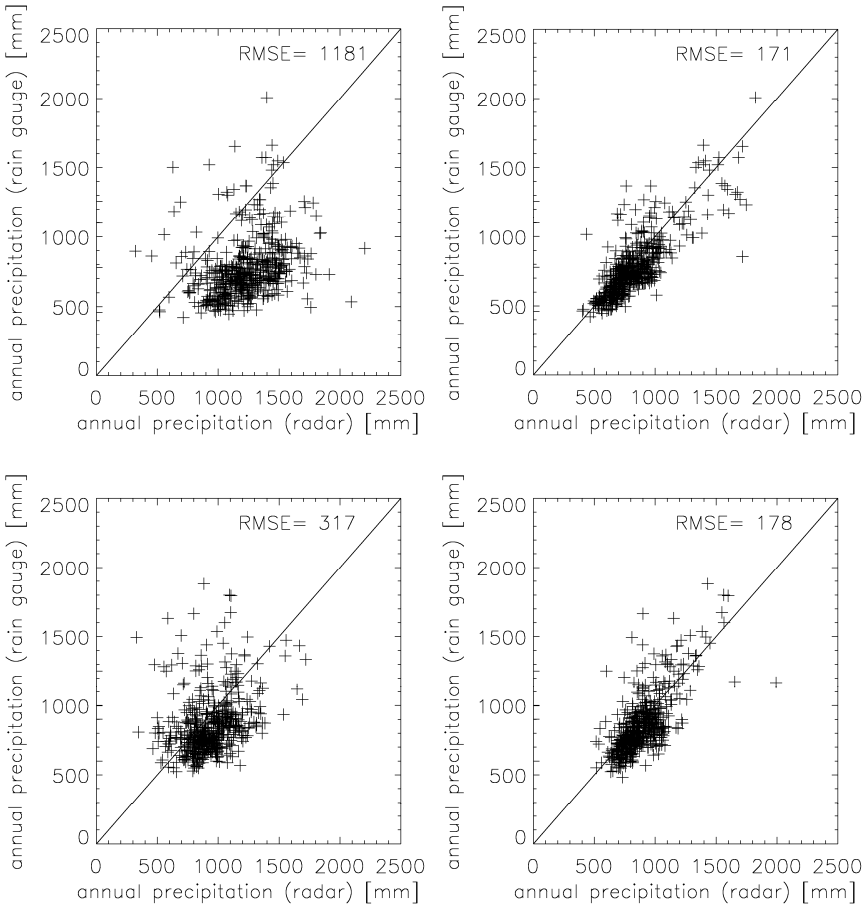

Figure 10. Scatterplots of radar and rain gauge pairs of values for the annual rain amounts before (left panels) and after the correction (right panels) of the RX radar product for the years 2005, 2006 and 2009 (top panels) and the years 2007 and 2008 (bottom panels).

HESSD
12, 1765–1808, 2015

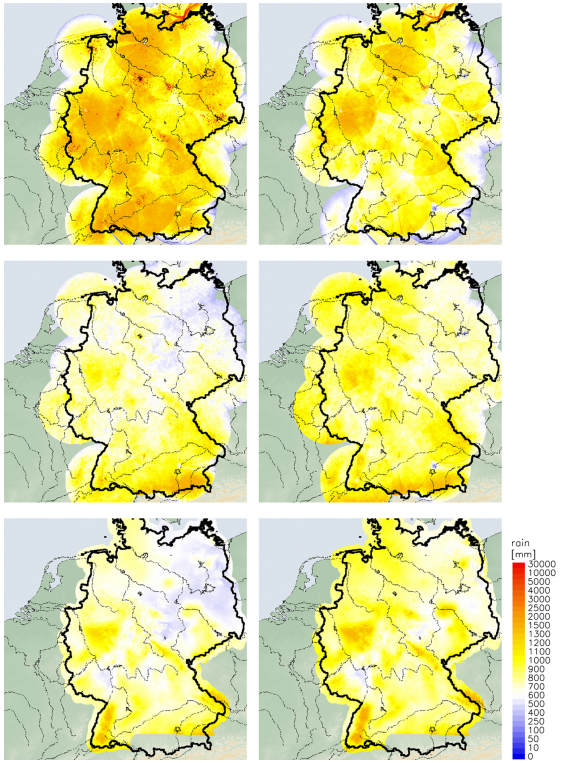

Figure 11. Annual rain amounts for Germany based on radar composite data RX for uncorrected radar data (top panels), corrected radar data (middle) and based on gauge data (bottom panels) for the years 2005, 2006 and 2009 (left panels) and for the years 2007 and 2008 (right panels).

HESSD
12, 1765–1808, 2015

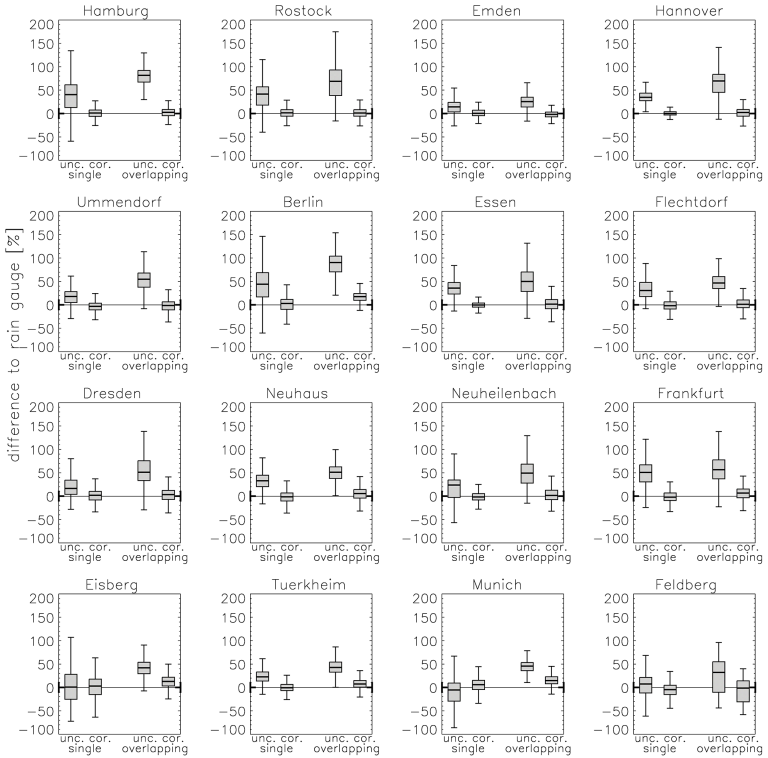

Figure 12. *Box*-and-*Whisker*-Diagrams of all corresponding pixels of Fig. 11 separated for each radar site for the time span 2005–2009. The percential difference between radar data and rain gauge is shown. The thick bar indicates the median of all differences. The boxes show the deviation of 50 % of radar and rain gauge pairs of values. The whiskers mark 1.5 times the corresponding interquartile range or, if not reached, the maximum deviation. The first two boxes of each diagram represent uncorrected and corrected pixels of the single radar of each radar site and the last two boxes are uncorrected and corrected pixels of corresponding overlapping areas.

HESSD
12, 1765–1808, 2015